

Effect of Laser-Focusing Conditions on Propagation and Monoenergetic Electron Production in Laser-Wakefield Accelerators

A. G. R. Thomas,¹ Z. Najmudin,¹ S. P. D. Mangles,¹ C. D. Murphy,^{1,2} A. E. Dangor,¹ C. Kamperidis,¹ K. L. Lancaster,² W. B. Mori,³ P. A. Norreys,² W. Rozmus,⁴ and K. Krushelnick¹

¹*Blackett Laboratory, Imperial College London, SW7 2AZ, United Kingdom*

²*Central Laser Facility, Rutherford Appleton Laboratory, Chilton, Oxon, OX11 0QX, United Kingdom*

³*University of California, Los Angeles, California 90095, USA*

⁴*Department of Physics, University of Alberta, Edmonton, Canada*

(Received 28 June 2006; published 1 March 2007)

The effect of laser-focusing conditions on the evolution of relativistic plasma waves in laser-wakefield accelerators is studied both experimentally and with particle-in-cell simulations. For short focal-length ($w_0 < \lambda_p$) interactions, beam breakup prevents stable propagation of the pulse. High field gradients lead to nonlocalized phase injection of electrons, and thus broad energy spread beams. However, for long focal-length geometries ($w_0 > \lambda_p$), a single optical filament can capture the majority of the laser energy and self-guide over distances comparable to the dephasing length, even for these short pulses ($c\tau \approx \lambda_p$). This allows the wakefield to evolve to the correct shape for the production of the monoenergetic electron bunches, as measured in the experiment.

DOI: [10.1103/PhysRevLett.98.095004](https://doi.org/10.1103/PhysRevLett.98.095004)

PACS numbers: 52.38.Kd, 41.75.Jv, 52.35.Mw

The concept of using lasers to accelerate particles to relativistic energies in plasma [1] has been brought closer to practical realization by recent experimental results. These have demonstrated the production of relativistic electron beams with high energies [2,3], low energy spread [4–6], and low emittance [7]. These accelerators promise to revolutionize the many uses of such particle beams, due to their high accelerating fields and thus compact size. Of the numerous laser-based schemes for plasma accelerators [1,8], only the laser-wakefield accelerator (LWFA) scheme has been capable of producing quasimonoenergetic electron beams [4–6]. The LWFA consists of a high intensity laser propagating through a plasma, such that the pulse length is shorter than the relativistic plasma wavelength ($c\tau \lesssim \lambda_p = 2\pi c/\omega_p$).

The longitudinal electric field of the wakefield—a relativistic electron plasma wave, with phase velocity $\beta_{ph}c$, generated by the ponderomotive force of the pulse—can be used to accelerate trapped electrons. The maximum electric field the wave can support, in the cold one-dimensional limit, is $E_{\max} = [2(\gamma_{ph} - 1)]^{1/2}E_0$, where $E_0 = m_e c \omega_p / e$ and $\gamma_{ph} = (1 - \beta_{ph}^2)^{-1/2}$ [9]. When the wave reaches this wave-breaking threshold, the maximum longitudinal velocity of plasma wave electrons exceeds $\beta_{ph}c$. Electrons are self-trapped and accelerated forward, instead of oscillating around their initial position.

In multiple dimensions, the self-trapping mechanism and the wakefield dynamics can be very different from the one-dimensional case [10–12]. In three dimensions, due to the large radial component of the electron trajectories, wake oscillations are heavily damped [13] to the extent that in the extreme case, there is only one plasma wave period [14]. Because of electron cavitation and ion inertia, the electric fields in this wave period are approxi-

mately linear and focusing towards the center of the ion cavity. Electrons slipping back with respect to the pulse are injected into the rear of the cavity where the electric field is strongly forward accelerating. If the charge in the injected bunch is high enough, its own electric field counteracts that of the cavitating region, preventing further injection and creating a short, monoenergetic bunch.

The electrons in the bunch can reach energies determined by the electric field in the plasma wave and the length over which the acceleration takes place. The maximum energy that an electron can gain is set by the dephasing length $L_D \approx \gamma_{ph}^2 \lambda_p$, which is the distance before the relativistic electrons outrun the accelerating phase of the wake [8]. For this to happen, the laser must propagate at high intensity to the order of L_D , which is generally longer than its Rayleigh length, z_R .

Because of the increased energy requirement and technical difficulty in producing intense, ultra-short pulses, initial LWFA studies used short focal-length optics to obtain high intensities in order to obtain wave breaking (a theoretical criteria for injection is that the laser normalized vector potential $a_0 = eA/m_e c > 4.3$ [12]). However, experimental results with tight focusing not using a guiding channel have been less successful in terms of charge, electron energy, and spectral shape than with longer focal-length focusing optics and $a_0 \approx 1$ [4,6].

In this Letter, we examine the importance of the focusing geometry on the evolution of plasma waves and laser pulse propagation in a LWF accelerator. This is done experimentally by directly comparing laser pulse and electron beam characteristics using two different focusing geometries, chosen to produce either a spot of size $w_0 < \lambda_p$ or $w_0 > \lambda_p$ for $c\tau \lesssim \lambda_p$. We demonstrate that for $w_0 > \lambda_p$, self-focusing permits a_0 to be sufficiently amplified to

allow self-injection. Moreover, the quasistatic nature of this compression allows for an adiabatic (i.e., controlled) approach to self-injection, which results in production of monoenergetic bunches. We also show that the pulse is maintained at high intensity, through self-guiding, over a distance $\sim L_D$, which is necessary for efficient acceleration of the bunch. With shorter focal-length focusing and $w_0 < \lambda_p$, the interaction is characterized by filamented laser propagation and excessive curvature of the plasma wave, resulting in broad electron spectra. The experimental observations are supported by a series of 2D particle-in-cell (PIC) code simulations.

The experiments were carried out on the Ti:Sapphire ASTRA laser which provided pulses of energy up to $E_L = 700$ mJ, pulse length $\tau = 50(\pm 5)$ fs FWHM at a central wavelength $\lambda_0 = 795$ nm. The laser was focused with either $f/3$ or $f/12$ off-axis parabolic mirrors, where the f refers to the ratio of focal length to initial diameter. The measured spot sizes (FWHM) at focus were $4 \mu\text{m}$ and $20 \mu\text{m}$, respectively, resulting in vacuum focused intensities of $5.5 \times 10^{19} \text{ W cm}^{-2}$ and $2.2 \times 10^{18} \text{ W cm}^{-2}$ corresponding to a_0 of 5 and 1. The M^2 of both focal spots was 2.6, giving $z_R (= \pi w_0^2 / M^2 \lambda_0)$ of $25 \mu\text{m}$ and $600 \mu\text{m}$, respectively. The laser pulses were focused ($z = 0$) onto the front edge of a 3 mm diameter conical helium gas-jet. This provided initial electron densities of $1 \times 10^{18} \text{ cm}^{-3} < n_e < 3 \times 10^{19} \text{ cm}^{-3}$.

The light transmitted through the plasma was measured after reflection by a glass plate, which served to attenuate the intensity and limit spectral modifications caused by the window of the target chamber. Light within a $f/5$ cone was collimated and re-imaged onto a 12 bit CCD camera. Light scattered at 90° to the direction of propagation was re-imaged both perpendicular and parallel to the laser polarization.

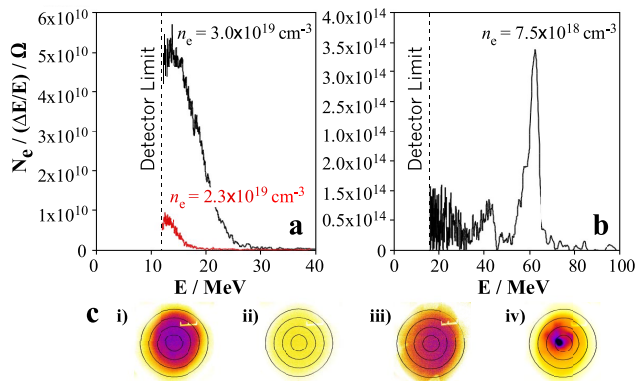


FIG. 1 (color online). Electron spectra for (a) $f/3$ at $n_e = 3.0 \times 10^{19} \text{ cm}^{-3}$ and $2.4 \times 10^{19} \text{ cm}^{-3}$. (b) $f/12$ at $n_e = 7.5 \times 10^{18} \text{ cm}^{-3}$. (c) Electron beam divergence measurements for (i) $f/3$, $n_e = 3.0 \times 10^{19} \text{ cm}^{-3}$, (ii) $f/3$, $n_e = 1.5 \times 10^{19} \text{ cm}^{-3}$, (iii) $f/12$, $n_e = 3.0 \times 10^{19} \text{ cm}^{-3}$, (iv) $f/12$, $n_e = 1.5 \times 10^{19} \text{ cm}^{-3}$. The circles denote ~ 10 mrad intervals.

The electron beam divergence was measured with a removable LANEX scintillating screen with a 5° opening angle. The energy spectrum of the accelerated electrons was obtained with a magnetic spectrometer with a 5×1 mm steel collimator, using image plate detectors. These have a linear response over a dynamic range of 10^8 , $50 \mu\text{m}$ spatial resolution, and allow calibrated, single-shot acquisition of the full spectrum [15]. Alternatively, for the high charge monoenergetic beams, a LANEX screen was used for high-repetition rate acquisition.

With both $f/3$ and $f/12$ focusing, at high density ($c\tau > \lambda_p$) quasi-Maxwellian electron energy spectra were observed with little shot-to-shot variation. This is indicative of self-modulation of the pulse [16], where the wakefield amplitude can reach the wave breaking threshold over multiple wave periods. This and the shorter dephasing length cause the large energy spread, Fig. 1(a) [4]. The divergence measurements show an almost uniform beam profile over an instrument limited opening angle of 5° , Fig. 1(c) (i) and (iii). Measurements taken with image plates closer to the interaction indicate that the actual divergence was significantly greater than this.

When $c\tau \lesssim \lambda_p$, the LWF regime is entered. In the case of the $f/3$ the number of accelerated electrons was dramatically reduced, Fig. 1(c) (ii). Coupled with the falloff in electron flux due to the high beam divergence, the spectrometer could no longer detect any electron signal above noise level, even with the sensitive image plates.

However, with $f/12$ focusing, monoenergetic spectra were observed in the range $5.6 \times 10^{18} \text{ cm}^{-3} \leq n_e \leq 2.0 \times 10^{19} \text{ cm}^{-3}$, Fig. 1(b). The electron beam divergence monitor consistently measured well collimated beams, with opening half-angle ≤ 5 mrad, Fig. 1(c) (iv). Large fluctuations in charge were measured by the electron spectrometer. This was due to a variation in electron beam pointing (3×10^{-3} sr) which was greater than the collection solid-angle of the electron spectrometer collimator (5×10^{-6} sr). This could also account for the observed variation in energy and energy spread. The ratio of the standard deviation to mean of the electron beam peak energy is $\sigma/\bar{E} = 0.18$, for 10 consecutive shots at $n_e = 7.5 \times 10^{18} \text{ cm}^{-3}$ with $\bar{E} = 80$ MeV.

Side scattered images of the interaction indicate that the short focal-length optic had a short interaction length ($\sim z_R$) while for the long focal-length, they indicate extended propagation. Figure 2 shows images of the transmitted light at 800 nm and $z = 2$ mm. With $f/3$ focusing at all densities within the experimental range, the pulse was broken up into multiple filaments [Fig. 2(a)], even when the power for relativistic self-focusing was exceeded, $P > P_{cr} = 17.3(\omega_0/\omega_p)^2 \text{ GW}$ [8]. As the density increased, the average filament size decreased.

The lack of guiding indicates why the $f/3$ ($w_0 < \lambda_p$) cannot produce reproducible monoenergetic electrons under these conditions. To produce monoenergetic electron

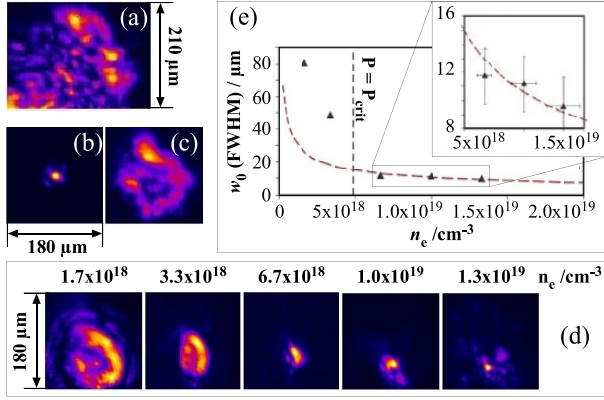


FIG. 2 (color online). Transmitted light at 800 nm imaged at $z = 2 \text{ mm}$ for (a) $f/3$, $n_e = 1 \times 10^{19} \text{ cm}^{-3}$ and (d) $f/12$ at various densities. Also shown is the $f/12$ spot in vacuum (b) at focus and (c) $z = 2 \text{ mm}$. (e) Mean spot width as a function of n_e . Vertical line is $P/P_{\text{cr}} = 1$; dotted line is $w_0 = \lambda_p$.

spectra, the laser must propagate for distances on the order of L_D . Because of the filamentation, it is unlikely that a single filament could efficiently trap sufficient energy to generate beams of high quality and charge [17] compared with those obtained using a long focal-length optic.

In contrast, using the $f/12$ optic [Fig. 2(d)], the pulse emerged as a single filament in the density range of monoenergetic electron spectra ($6.7\text{--}13 \times 10^{18} \text{ cm}^{-3}$). The spatial extent was comparable to that of the laser focus and scales with λ_p [Fig. 2(e)], indicating that the pulse has self-guided for a distance $\sim 2 \text{ mm}$. The observed extended propagation allows the necessary nonlinear pulse modification for injection of a single monoenergetic bunch of electrons. Measurements of the transmitted energy suggest that at this point, the pulse has depleted to below a sufficient power to maintain self-guiding. This is in contrast to the $f/3$ case, where almost all of the energy is transmitted.

For $n_e > 2 \times 10^{19} \text{ cm}^{-3}$, the spatial extent was large again. Depletion is so severe ($> 10 \times$) that self-guiding cannot be maintained over this length. At the lowest densities ($1.7\text{--}3.3 \times 10^{18} \text{ cm}^{-3}$), for which $P/P_{\text{cr}} < 1$, the spatial extent of the filament was close to that in vacuum at $z = 2 \text{ mm}$. This indicates that self-focusing only partially compensates for diffraction in this case.

To our knowledge, these measurements are the first evidence for self-guided propagation of short pulses ($c\tau \approx \lambda_p$). Note that previous results that suggested self-focusing is ineffective in this regime, only considered a short focal-length geometry ($w_0 \ll \lambda_p$) [18].

The two configurations were simulated using the 2D PIC code OSIRIS on an eight node Macintosh G5 cluster. The simulations were run with similar parameters to the experiments, at 4 particles/cell using a grid of up to 1500×6000 (> 18 cells/ λ in x and up to > 18 cells/ λ in y). A Gaussian focus was used, due to the difficulty of initializing a realistic focus. The embedded Gaussian of the experimen-

tal focus was modeled to obtain similar diffraction and Rayleigh lengths. This corresponds to $w_0 = 2$ or $10 \mu\text{m}$. w_0 is defined as the half width at $1/e^2$ maximum at vacuum focus. Simulations with intermediate focusing geometries were also performed. The density profile consisted of a $300 \mu\text{m}$ linear ramp followed by a plateau of density n_{e0} , to approximate the measured profile. The vacuum focus ($z = 0$) was at the start of the plateau.

Directly after focus, the $2 \mu\text{m}$ pulse develops a complex, strongly time-dependent mode structure. This elicits a plasma response that enhances the structure via the self-focusing instability and evolves to a multifilament structure [Fig. 3(a)] reminiscent of the analytical solution [19] in the stationary approximation. Only about 30% of the pulse energy is trapped in a central filament.

By contrast, the $10 \mu\text{m}$ pulse focuses radially and compresses temporally, capturing almost all of the initial pulse energy [Fig. 3(c)]. The average pulse half-width shrinks to $\approx 4 \mu\text{m}$, and the pulse propagates at this width for longer than z_R , until it is depleted. Unlike the $2 \mu\text{m}$ case, the propagation is quasistatic, and self-focusing occurs on a longer time scale.

Electron density plots are also shown [Fig. 3(d) and 3(e)] for both $2 \mu\text{m}$ and $10 \mu\text{m}$ simulations at the point where the plasma wave amplitude approaches its maximum value. Note that this amplitude maximum is at very different points in the simulation for the two pulses. Overlaid are contours of the laser a_0 , showing how the electron density profile directs the laser energy.

The $2 \mu\text{m}$ pulse interaction is shown close to focus, after which it breaks up, and the wake amplitude decreases. Electrons from the edge of the pulse are attracted axially by the ion cavity produced by the intense pulse. The distance to reach axis should be similar to the distance the electrons slip back in the speed of light frame in this time, as they are relativistic. However, the pulse length in the case of the

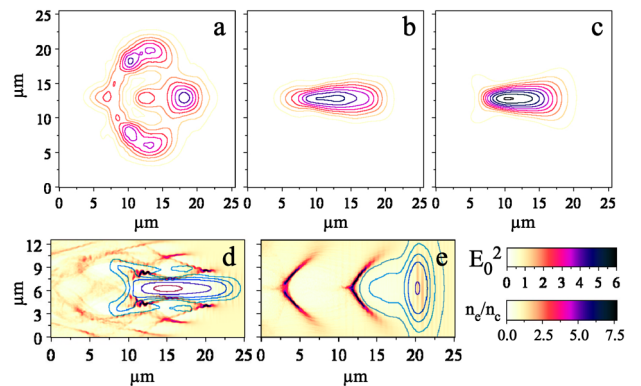


FIG. 3 (color online). Simulations with $E_L = 500 \text{ mJ}$, $\tau = 40 \text{ fs}$, $n_e = 2 \times 10^{19} \text{ cm}^{-3}$, showing: Contour plots of the laser envelope $(eE/mc\omega_0)^2$ for $w_0 =$ (a) 2 , (b) 6 , and (c) $10 \mu\text{m}$ at $z = 2z_R$; n_e plotted for (d) $w_0 = 2 \mu\text{m}$ at $z = 0$, (e) $w_0 = 10 \mu\text{m}$ at $z = 3z_R$. Overlaid are laser contours at $a = 1, 1.5, 2, 3, 4$.

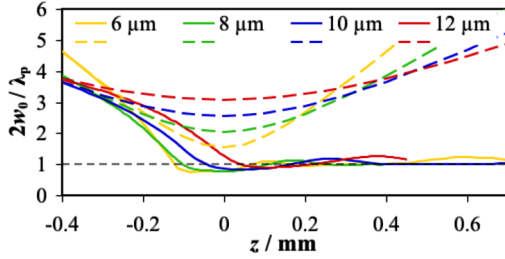


FIG. 4 (color online). Simulated temporal evolution of spot diameter at $1/e^2$ ($2w$), with various focusing geometries for $n_{e0}/n_c = 0.01$, $P/P_{cr} = 2$. Vacuum foci are at $z = 0 \mu\text{m}$. Solid lines indicate simulated propagation. Dashed lines show theoretical propagation for a Gaussian pulse in vacuum.

$f/3$ is much greater than its waist. Hence, the electrons move into the pulse envelope before being repelled by the ponderomotive force of the laser, as in Fig. 3(d), which causes the breakup of the pulse.

The $10 \mu\text{m}$ pulse produces an initially more gently curved wake and reaches maximum amplitude later after nonlinear modulation has increased its intensity. Even when the intensity is raised so that electron cavitation occurs quickly, there is still no breakup of the pulse as the width is similar to the pulse length.

A scan in waist (between 1 and $14 \mu\text{m}$) was simulated at $n_{e0}/n_c = 0.01$, corresponding to $0.14 < w_0/\lambda_p < 2$, for a fixed equivalent power, $P = 13 \text{ TW}$. As noted above, larger ($\geq 6 \mu\text{m}$) focal spots show stable quasistatic propagation [Fig. 3(b) and 3(c)], while spot sizes $< 4 \mu\text{m}$ [Fig. 3(a)] show beam breakup and dynamical self-focusing. Intermediate focusing geometries ($\sim 4 \mu\text{m}$) show evidence of a transition region between the two regimes.

An intensity scan ($I_0/4 \leq I \leq 4I_0$) at fixed density and a density scan $0.005 \leq n_{e0}/n_c \leq 0.02$ at fixed intensity were also simulated for both $2 \mu\text{m}$ and $6 \mu\text{m}$ geometries. The simulations were qualitatively invariant for both focusing geometries in this parameter range. The simulations also show that the pulse tends to self-focus to a diameter $2w_0 \approx \lambda_p$ and oscillate around an equilibrium position (Fig. 4). This is independent of the initial f number, provided $w_0 \gtrsim \lambda_p$.

Despite the short pulse duration, a simple stationary envelope treatment [20] can be used. For $a_0 \gg 1$, the spot size w obeys $\partial^2 \bar{w} / \partial t^2 = V_0(1/\bar{w}^3 - 16\sqrt{2}P/P_{cr})$ for a linearly polarized laser. Here, $V_0 = [(c\lambda_0/\pi)/(w_0^2 a_0^2)]^2$, $\bar{w} = w/w_0 a_0$. Self-focusing will therefore start to dominate diffraction ($\partial^2 \bar{w} / \partial t^2 = 0$) for $w/\lambda_p = (\frac{1}{4}P/P_{cr})^{1/6}/\pi$. Hence, for a mildly relativistic pulse, e.g., $P/P_{cr} \approx 2$, the matched spot size $2w \approx (2/3)\lambda_p$. This is in reasonable agreement with the simulations, the discrepancy being due to the assumptions of constant density and the $a_0 \gg 1$ approximation. For tight focusing geometries and high

intensities where $w_0 \lesssim \lambda_p$ and for $a_0 \gg 1$, complete electron blowout can occur [14] and a nonadiabatic kinetic analysis of self-focusing is required.

In conclusion, we have demonstrated the self-guiding of an ultrashort laser pulse ($c\tau \sim \lambda_p$) provided the vacuum spot-size $w_0 \gtrsim \lambda_p$. Pulses with vacuum spot size greater than this can propagate many z_R , oscillating about a matched spot size. However, focusing to smaller than $\sim \lambda_p$ will result in mode structures, which through self-focusing seeded beam breakup prevent production of high quality electron beams. So for reproducible production of monoenergetic electron, the ratio of pulse length to spot size should be $\lesssim 1$. To overcome low laser powers, increasing pulse intensity through pulse compression and photon deceleration of the leading edge [12] is more effective than focusing more tightly. Careful choice of spot size, striking a balance between pump depletion with large f numbers and filamentation at low f numbers, will increase the efficacy of the interaction. This competition between over and under-focusing will be important even at higher intensities and so necessitates a careful choice of focusing conditions in future experiments.

This work was supported by EPSRC, Alpha-X, and the US DOE. The authors acknowledge the staff of the CLF (RAL) for technical assistance and the OSIRIS consortium (UCLA/IST/USC) for the use of OSIRIS.

-
- [1] T. Tajima and J.M. Dawson, Phys. Rev. Lett. **43**, 267 (1979).
 - [2] S. P. D. Mangles *et al.*, Phys. Rev. Lett. **94**, 245001 (2005).
 - [3] V. Malka *et al.*, Science **298**, 1596 (2002).
 - [4] S. P. D. Mangles *et al.*, Nature (London) **431**, 535 (2004).
 - [5] C. G. R. Geddes *et al.*, Nature (London) **431**, 538 (2004).
 - [6] J. Faure *et al.*, Nature (London) **431**, 541 (2004).
 - [7] S. Fritzler *et al.*, Phys. Rev. Lett. **92**, 165006 (2004).
 - [8] E. Esarey *et al.*, IEEE Trans. Plasma Sci. **24**, 252 (1996).
 - [9] A. I. Akhiezer and R. V. Polovin, Sov. Phys. JETP **3**, 696 (1956).
 - [10] S. V. Bulanov *et al.*, Phys. Rev. Lett. **78**, 4205 (1997).
 - [11] S. Gordienko and A. Pukhov, Phys. Plasmas **12**, 043109 (2005).
 - [12] F. S. Tsung *et al.*, Phys. Rev. Lett. **93**, 185002 (2004).
 - [13] J. M. Dawson, Phys. Rev. **113**, 383 (1959).
 - [14] A. Pukhov and J. Meyer-ter-Vehn, Appl. Phys. B **74**, 355 (2002).
 - [15] Y. Iwabuchi *et al.*, Jpn. J. Appl. Phys. **33**, 178 (1994).
 - [16] P. Sprangle *et al.*, Appl. Phys. Lett. **53**, 2146 (1988); N. Andreev *et al.*, JETP Lett. **55**, 571 (1992).
 - [17] B. Hidding *et al.*, Phys. Rev. Lett. **96**, 105004 (2006).
 - [18] C. Delfin *et al.*, Phys. Plasmas **9**, 937 (2002); J. Faure *et al.*, Phys. Plasmas **9**, 756 (2002).
 - [19] F. Cattani *et al.*, Phys. Rev. E **64**, 016412 (2001); X. Wang *et al.*, Phys. Rev. Lett. **84**, 5324 (2000).
 - [20] P. Sprangle *et al.*, IEEE Trans. Plasma Sci. **15**, 145 (1987).